Biosensors and Bioelectronics 143 (2019) 111636

Contents lists available at ScienceDirect

Biosensors and Bioelectronics

journal homepage: www.elsevier.com/locate/bios

Sensitive detection of ketamine with an electrochemical sensor based on UV-induced polymerized molecularly imprinted membranes at graphene and MOFs modified electrode

Kaixin Fu[a], Ruilin Zhang[b], Jingcheng He[a], Huiping Bai[a,*], Genlin Zhang[a,**]

[a] School of Material Science and Technology, Yunnan Key Laboratory of Micro/Nano Materials & Technology, Yunnan University, Kunming, 650091, China
[b] Institut of Forensic Medical, Kunming Medical University, Kunming, 650050, China

ARTICLE INFO

Keywords:
Ketamine
Molecularly imprinted sensor
MOFs@G nanocomposite
UV-Induced
Screen printed electrode

ABSTRACT

Ketamine is one of the most widely abused drugs in the world and poses a serious threat to human health and social stability; therefore, the ability to accurately monitor the substance in real-time is necessary. However, several problems still exists towards this goal, such as the generally low concentration of the target molecules disturbed in the complex samples that undergo analysis during criminal investigations. In this work, the sensitive and selective detection of ketamine was accomplished by molecularly imprinted electrochemical sensor. The molecularly imprinted membrane as a biomimetic recognition element was fabricated by the UV-induced polymerization of methacrylic acid (MAA) and ethylene glycol dimethacrylate (EGDMA) on a metal-organic framework/graphene nanocomposite (MOFs@G) modified screen-printed electrode. The screen printed electrode (SPE) provided good adhesion for the formation of the imprinted membranes and increased the stability of the sensor. The morphology and performance of the imprinted films were characterized in detail by scanning electron microscopy (SEM), cyclic voltammetry (CV), electrochemical impedance spectroscopy (EIS), and differential pulse voltammetry (DPV). The experimental results demonstrated that the imprinted sensor had excellent sensitivity, selectivity, and long-term stability. It offered a low detection limit (4.0×10^{-11} mol L^{-1}) and had a dynamic range from 1.0×10^{-10} mol L^{-1} to 4.0×10^{-5} mol L^{-1}. Furthermore, the established method was successfully applied for the determination of ketamine in urine and saliva samples.

1. Introduction

Ketamine (KT), the main constituent of “K Powder”, a well-known anesthetic drug used in medical science that produces a wide range of sedative effects (Favretto et al., 2013). Ketamine is normally odorless, tasteless and colorless. It can be easily added to beverages without being perceived by the victim, and results in stupor and sedation along with amnesia (Yang et al., 2019; Shawish et al., 2014). Because of its hallucinogenic and euphoric potential, the drug was abused in the United States shortly after it began marketing in the 1970s; it became popular among young users at dance and rave parties, and is one of the recreational drugs known as “club drugs”. Ketamine addiction is a common worldwide problem (Maddah et al., 2015; Leung et al., 2016). Given the broad potential for abuse, the sensitive detection of ketamine is essential for clinical diagnosis and law enforcement.

Gas chromatography-mass spectrometry (GC-MS) (Lian et al., 2012; Moreno et al., 2015), liquid chromatography-mass spectrometry (LC-MS) (Peng et al., 2019; Ramiole et al., 2017), capillary electrophoresis (Porpiglia et al., 2016), and electrochemical methods (Chen et al., 2013; Deiminiat and Rounaghi, 2018; Narang et al., 2017) are the common analytical methods used for ketamine detection. While mass spectrometry is universally used, the method is not portable and requires several laborious sample preparation steps. Moreover, most of these methods require sample manipulation, which makes them vulnerable to various interferences; in addition, they cannot be used for colored and turbid solutions (Shawish et al., 2014, 2015). Electrochemical sensors have many advantages such as a high sensitivity, selectivity, and real-time chemical analysis. Several reported electrochemical methods based on ion-selective electrodes (Shawish et al., 2014; El-Naby, 2014), immune analysis (Chen et al., 2013), or molecular imprinted technology (Deiminiat and Rounaghi, 2018) can be considered as good alternatives because of their attractive

* Corresponding author.
** Corresponding author.
E-mail addresses: baihuiping@ynu.edu.cn (H. Bai), zhanggenlin@ynu.edu.cn (G. Zhang).

https://doi.org/10.1016/j.bios.2019.111636
Received 13 May 2019; Received in revised form 21 August 2019; Accepted 26 August 2019
Available online 28 August 2019
0956-5663/

characteristics mentioned above. However, the detection limit of ion-selective electrodes needs to be further reduced (Shawish et al., 2014); immunoassays have a high specificity and sensitivity, but they also have some weakness, such as a dependence on animals, long preparation time, high costs, and difficult storage.

Molecularly imprinted polymers (MIPs) are a kind of functional material, and have attracted a significant amount of attention in recent years. MIPs have unique advantages over natural biological receptors in terms of their physical and chemical stability, ease of preparation, low cost, and applicability in harsh environmental conditions. Moreover, an important aspect of MIPs is their highly selective characteristics due to its potential for selectively binding to target compounds (Ahmad et al., 2019; Ayankojo et al., 2018). Molecularly imprinted electrochemical sensors (MIECS) combine the specific recognition abilities of MIPs and the high sensitivity of electrochemical detection. They can be easily miniaturized and automated for operation at a low cost (Li et al., 2013; Ahmad et al., 2019).

Urine samples continue to be widely used as a biological matrix for the analysis of drugs because it is an easily-accessible bodily fluid that provides metabolic information. Ketamine is mainly present in urine in the form of protoplast (Theurillat et al., 2007). However, the complicated composition of urine generally negatively effects the detection of drugs in real human urine; therefore, MIPs were introduced to separate and collect the constituent target molecules in human urine, for selective detection.

The sensor's sensitivity is an important factor for evaluating its validity. Here, graphene and metal-organic frameworks (MOFs) nanomaterials have been applied as substrates to improve the sensitivity of MIECS. Graphene (G), is a two-dimensional single layer carbon material that has shown potential in the field of sensor devices because of its excellent properties, such as a large surface area, good chemical stability, and high electrical conductivity (Ghanei-Motlagh et al., 2016). Research suggests that the use of graphene can effectively improve the sensitivity of sensors (Bai et al., 2015; Taniselass et al., 2019). However, the graphene has poor dispersion of in solvents, and is prone to aggregate. Aim at this problem, MOFs with strong adsorption properties was introduced. The dispersion of graphene can be significantly improved in water by compounding with MOFs. MOFs, as crystalline porous inorganic polymers, are usually formed by the coordination polymerization of metal ions and certain organic linkers (Furukawa et al., 2013; Liu et al., 2018). The inherent advantages of MOFs include their high porosity and specific surface area, which result in an excellent adsorption capacity and mass transfer rate that makes them superior to traditional MIP supports. These properties make MOFs an ideal support material (Liu et al., 2018). The resulting MIPs have been reported in MOF-based sensors such as in electrochemical sensors, optical sensors, and also as a quartz crystal micro-balance sensor with improved sensing selectivity (Bagheri et al., 2018; Guo et al., 2016).

In order to achieve rapid separation and determination of ketamine in human urine, we developed a highly selective, sensitive, and stable electrochemical sensor based on a graphene and MOF modified screen printed electrode. High selectivity is obtained by molecular imprinting and high sensitivity is achieved through the dual-signal amplification effects of graphene and MOFs. The MOFs@G enhanced the surface area of the imprinted membranes and increased the number of effective binding cavities. Screen printed electrodes (SPE) are a kind of disposable composite electrode that has a relative rough surface and does not need any complex pretreatment (Chen et al., 2018). It provides good adhesion for the formation of imprinted membranes. In particular, SPE is affordable, user-friendly, affords easy integration, and is convenient for large-scale application compared to conventional metal electrodes such as glassy carbon and gold electrodes. Consequently, this sensor showed better results in terms of linearity, detection limits, and selectivity to ketamine in complex biological samples.

2. Experimental

2.1. Apparatus and instruments

All electrochemical data were carried out with a CHI760E electrochemical workstation (Shanghai CH Instruments Co., China). The electrochemical impedance spectroscopy (EIS) data was performed on Autolab302N (Metrohm, Netherlands). SPE obtained from Suzhou Mayor Triangle System Biological Cross Science Research Institute Co., Ltd. (Suzhou, China) was employed as the integrated electrode ($30 \times 10 \times 0.25$ mm). The surface morphology was observed on a Hitachi S520 field emission scanning electron microscopy (Tokey, Japan).

2.2. Reagents and chemicals

Ketamine hydrochloride, norketamine (NKT), methylenedioxy methamphetamine (MDMA), methylamphetamine (MA) were obtained from Kunming Medical University (Kunming, China). Acrylamide (AM), methacrylic acid (MAA), 2-acetamidoacrylic acid (AAA) and 2-(allylmercapto) nicotinic acid (ANA) were purchased from Sigma Aldrich (USA). Ethylene glycol dimethacrylate (EGDMA) was purchased from Suzhou Anli Chemical Factory (Jiangsu, China) and distilled under vacuum to remove the stabilizers prior to use. Azobisisobutyronitrile (AIBN) was purchased from Shanghai Reagent Factory (Shanghai, China) and purified by recrystallization from ethanol before used. Zirconium chloride ($ZrCl_4$, 98.0%), 1,4-benzendicarboxylicacid (BDC, analytical grade), N,N-dimethylformamide (DMF, > 99.8%), dopamine (DA) and ascorbic acid (Vc) were supplied by Sinopharm Chemical Reagent CO., Ltd., China. The reagents and solvents used without special illustration were analytically pure grade and used without further purification.

2.3. Synthesis of MOFs

The Zr-MOF was synthesized according to a reported method with some modification (Cavka et al., 2008). $ZrCl_4$ and BDC were dissolved in DMF with a molar ratio of 1:1:500 under continuous stirring. Following this, the mixture was transferred to a 100 mL Teflon-lined autoclave and heated at 120 °C for 48 h. After cooling to room temperature, the solid products were collected by centrifugation, washed with methanol, and dried (24 h, 120 °C) under vacuum.

2.4. Preparation of the MOFs@G modified electrode

The SPE was rinsed with deionized water several times under ultrasonication. Then, it was immersed in a 0.05 M H_2SO_4 solution and scanned for several cycles using cyclic voltammetry from 0.50 V to 1.10 V at 100 mV s^{-1} under stirring until a stable voltammogram was observed.

Graphene (G) was prepared according to previously reported literature from our group (Bai et al., 2015). 1.0 mg of the prepared MOFs and 1.0 mg of G were dispersed in 2.0 mL of ethanol and ultra-sonicated for 1 h to obtain a homogenous suspension (1.0 mg mL^{-1}). Following this, 2.0 μL of the suspension was dropped onto the surface of a freshly prepared screen printed electrode and dried under an infrared lamp to finally obtain the modified MOFs@G/SPE.

2.5. Preparation of the KT-imprinted and non-imprinted membrane modified electrode

The KT-imprinted membrane (MIM) and non-imprinted membrane (NIM) were prepared via the UV-triggered polymerization method. First, 0.0125 mmol of ketamine was dissolved in 30 μL of methanol, and then, 0.05 mmol of MAA and 0.47 mL of acetonitrile were added. After ultrasonication for 5 min and pre-polymerization for 30 min, 0.5 mmol

of EGDMA and 0.04 mmol of AIBN were added to the mixture to prepare the polymerization solution. Next, 2.0 μL of the above solution was dropped onto the surface of MOFs@G/SPE and the polymerization process proceeded under UV exposure (380 nm) for 3 h. After that, the electrode was first cooled in a refrigerator, and then immersed in 1:9 (v/v) of acetic acid/methanol for 10 min to remove KT from the imprinted membrane. A non-imprinted membrane modified sensor (NIM/MOFs@G/SPE) was prepared under the same conditions in the absence of KT. All the sensors are stored in the refrigerator when not in use.

2.6. Electroanalytical measurements

The concentration of KT could be determined indirectly using $[Fe(CN)_6]^{3-/4-}$ as the medium. Cyclic voltammetry (CV) between −0.2–0.6 V at a scan rate of 100 mVs^{-1} in a 0.1 mol L^{-1} KCl solution containing 5.0 mmol L^{-1} $K_3[Fe(CN)_6]$ was applied for characterization of the electrode surface after each step of the modification. The electrochemical impedance spectroscopy (EIS) experiments were carried out under potential of 0.2 V, amplitude of 10 mV, and in the frequency range of 0.1–10^5 Hz. The differential pulse voltammetry (DPV) was recorded in the potential scan range from −0.2 to 0.6 V and with an amplitude, pulse width, sampling width, pulse period, and quiet time of 0.05 V, 0.05 s, 0.0167 s, 0.1 s, and 10 s, respectively. After each experimental run, the sensor was washed by immersion in 1:9 (v/v) acetic acid/methanol for 10 min to remove any KT on the electrode surface. The electrode could be reused after this cleaning procedure.

3. Results and discussion

3.1. Characterization of the MOFs@G and imprinted film

The surface morphology of the MOFs, graphene, and the ketamine molecular imprinted film were characterized by scanning electron microscopy (SEM). The crystal structures of the Zr-MOFs were determined by X-ray diffraction (XRD) analysis. As depicted in Fig. 1a, the Zr-MOFs have a regular polyhedron structure and the diameter of the particles is about 20–30 nm, which is in agreement with the reported literature (Zhang et al., 2018). Fig. 1 (b) shows that the Zr-MOFs exhibit typical XRD patterns. The characterization results show that the Zr-MOFs had been successfully prepared.

Fig. 1 (c) shows an SEM image of the MOFs@G composite modified on the SPE surface. It can be clearly seen that graphene exhibits a flake-like shape with a wrinkled surface morphology, and many of the MOF nanoparticles are coated on the graphene surface. It is obvious that the MOFs@G-modified electrode has a three-dimensional structure. This allows it to provide more surface area for the imprinted film, and more effectively promote electron transfer between the target molecules and the electrode. Meanwhile, graphene and MOFs exhibit the better disperse ability after compounding. The ethanol solution of MOFs@G composite is more homogeneous and stable than that of graphene under the same concentration (Fig. 1S) due to the introduction of MOFs. As shown in Fig. 1 (d), almost all the MOFs@G are decorated with MIPs films and the surface is smooth and homogeneous after the UV-induced polymerization. This indicates that the imprinted sites are generated in the MOFs@G hybrids. After elution, the surface of the MIM/MOFs@G becomes rough and porous, and displays a superior three-dimensional structure (Fig. 1 (e)). Compared to the imprinted membrane, the non-imprinted membrane is more compact after elution and only the superfluous polymer was removed (Fig. 1 (f)).

3.2. Electrochemical characterization

To further confirm the electrochemical characteristics of the MIM/MOFs@G/SPE sensor, cyclic voltammetry (CV), differential pulse voltammetry (DPV) and alternating current impedance (EIS) were both used in the 5.0 mmol L^{-1} $K_3Fe(CN)_6$ solution containing 0.1 mol L^{-1} KCl. As can be seen from Fig. 2A, compared to the bare electrode (curve a), the redox peak current of the nanocomposite modified electrode increase remarkably (curve b); this proves that the MOFs@G nanocomposite has good electrical conductivity and a high surface-to-volume ratio. However, after the formation of the non-conducting imprinted film on the surface of the MOFs@G modified electrode, the ferricyanide redox peaks disappeare (curve c); subsequently, a pair of redox peaks reappear after the removal of KT from the imprinted membrane (curve d); the results show that the imprinted cavities produced after elution can promote the redox reaction of the $[Fe(CN)_6]^{3-/4-}$ ion pair on the sensor surface. On the contrary, redox peak currents decrease from curve (d) to curve (curve e), the most probable reason is that the cavities in imprinted membrane were occupied by imprinting molecules KT after rebinding step, which hindered the electron transfer. The DPV responses on different electrodes were also recorded (Fig. S2). The result is consistent with the CVs, and further certifies that the synthesis process of the electrodes.

Fig. 2B shows the typical EIS spectra of different modified electrodes. The semicircle portion at higher frequencies in the EIS spectrum corresponds to the electron transfer resistance (R_{ct}). As expected, the EIS behaviors of the electrodes are similar to the voltammetric responses. The R_{ct} is almost zero, while the SPE (R_{ct} = 486 Ω) is modified for the MOFs@G nano-composite. The largest R_{ct} (9,895Ω), which is obtained for MIM/MOFs@G/SPE, is significantly decrease after the removal of the imprinted KT (R_{ct} = 1102 Ω); it then conversely enlarge after the rebinding of KT (R_{ct} = 1506 Ω). The EIS results further demonstrates the successful construction of the imprinted sensor and its binding ability.

3.3. Optimizing the constituents of the KT-imprinted membrane

3.3.1. Selection of functional monomer

The selectivity of the molecularly imprinted polymer is affected by the interaction between the template and the functional monomer. Therefore, we used UV spectrophotometry to investigate the interaction between the template ketamine molecule and four functional monomers (MAA, AM, ANA and AAA) in the polymerization period.

UV analysis shows that a clear ketamine absorption peak appears at 202 nm. The absorption peaks show a red shift together with a hyperchromicity effect on the addition of the different functional monomers (Fig. 3). The observed phenomenon arises due to the effects of hydrogen bonding on the first π-π* absorption band of the chromophore as a proton donor. The strongest change is obtained by adding MAA, which indicate that the interaction between KT and MAA is the strongest compared to the interaction of KT with the other monomers. A possible reason is that MAA is a typical H-bond donor and is also a functional acidic monomer, while KT is a typical H-bond receptor and an alkaline molecule. Hence, they can not only produce strong electrostatic interactions, but also form stable H-bonds. Therefore, MAA was chosen as the functional monomer for the polymerization.

3.3.2. Optimization of the molar ratio of the template, monomer, and the cross-linking agent

The molar ratio of the template, monomer, and the cross-linking agent would affect the quantity of the imprinted recognition sites in the molecularly imprinted membranes, the film formation, and the elution effects (Gam-Derouich et al., 2012); therefore, the DPV responses of the imprinted film modified electrodes with different polymerization molar ratios were investigated (Table 1S).

It could be seen that the electrode has maximum response sensitivity to KT, when the molar ratio of KT, MAA, and EGDMA is 1:4:40. The DPV response decrease when the ratio of the functional monomers is above or below 4. This may be because an insufficient amount of monomer results in a poor yield of imprinted sites, while a large monomer excess can induce a high cross-linking degree and make the recognition sites inaccessible. When the molar ratio of KT/EGDMA is

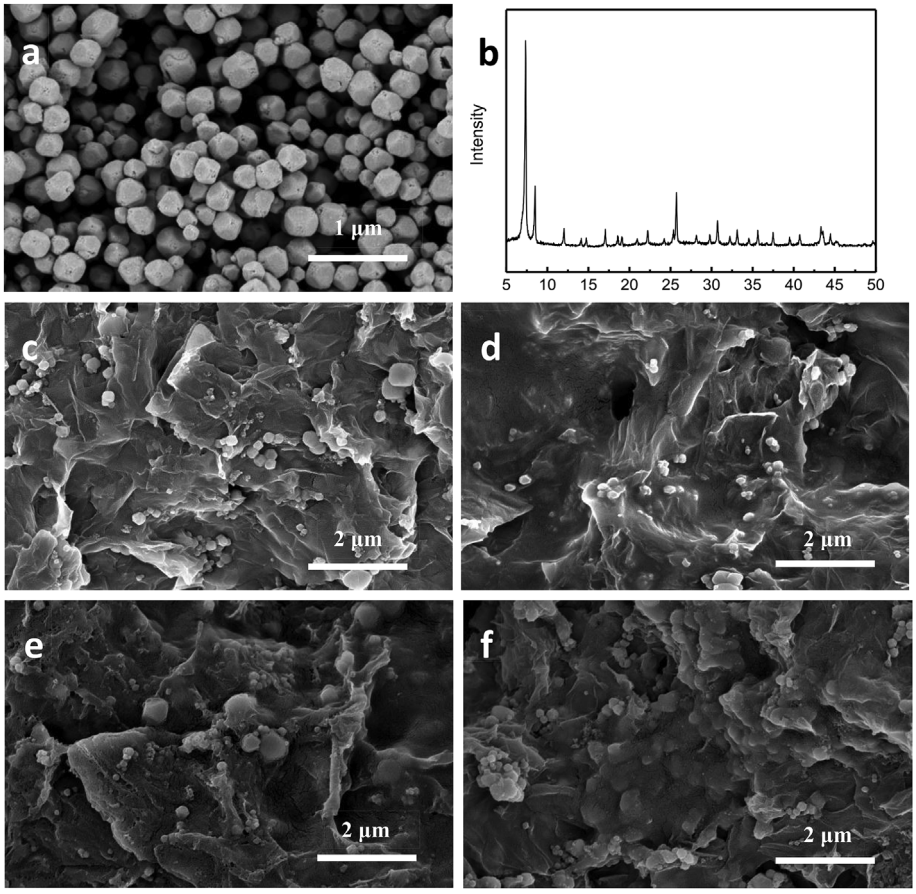

Fig. 1. SEM (a) and XRD (b) of MOFs, and SEM photographs of MOFs@G/SPE (c), KT-MIM/MOFs@G/SPE before (d) and after (e) template removal, NIM/MOFs@G/SPE after leaching process (f).

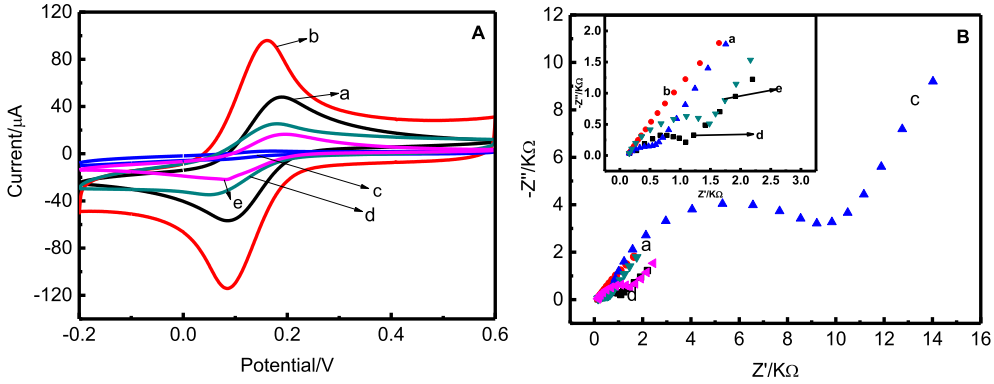

Fig. 2. (A) Cyclic voltammograms and (B) electrochemical impedance spectroscopy recorded in 5.0 mmol L^{-1} $K_3Fe(CN)_6$ and 0.1 mol L^{-1} KCl for (a) bare SPE, (b) MOFs@G/SPE, (c) KT-MIM/MOFs@G/SPE before template removal, (d) KT-MIM/MOFs@G/SPE after template removal, (e) KT-MIM/MOFs@G/SPE after rebinding.

1:20, it became difficult to form a stable imprinted polymer film on the MOFs@G modified SPE by UV irradiation. Furthermore, excessive cross-linking agent could lead to difficulty in removing template molecules from the imprinted film. In this work, the sensors were prepared with an optimal KT:MAA:EDGMA molar ratio of 1:4:40.

3.3.3. Optimizing the elution conditions

For the formation of the ketamine molecule imprinted membrane, the main binding force between the template and the functional monomer was the H-bond: therefore, a mixture of methanol and acetic acid (9:1, v/v) was selected as the optimal eluent to remove the template from the imprinted membrane. Under these conditions, ketamine could be removed from the imprinted membrane within 10 min, and the membrane maintained its integrity and stability.

3.4. Optimization of detection conditions

To evaluate the effect of the buffer solution, the response currents of KT on the sensors were examined in the following solutions: (1) 0.2 mol L^{-1} PBS (pH 7.0) with 5.0 mmol L^{-1} $K_3Fe(CN)_6$, (2) 0.2 mol L^{-1} of NaAc-HAc (pH 5.2) with 5.0 mmol L^{-1} $K_3Fe(CN)_6$, and (3) 0.1 mol L^{-1} KCl with 5.0 mmol L^{-1} $K_3Fe(CN)_6$ (pH 6.0). A high and stable response was obtained in 0.1 mol L^{-1} KCl. Meanwhile, the effects of the pH range from 4.0 to 9.0 on the sensor responses using 0.1 mol L^{-1} KCl (adjusting the pH with 0.1 mol L^{-1} HCl or NaOH) were investigated. The experimental result indicated that pH below 5.0 or

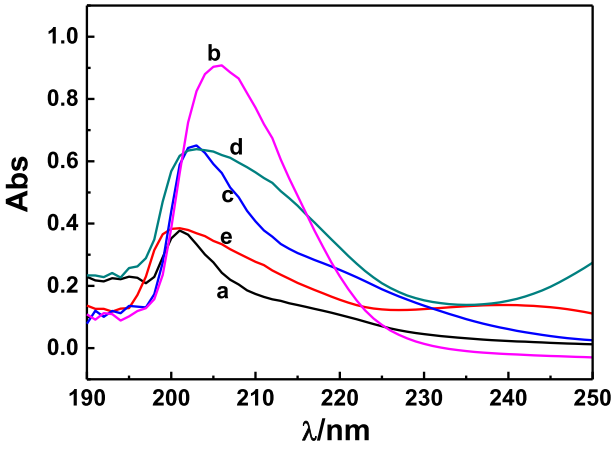

Fig. 3. The UV spectra of KT in the absence (a) or presence of function monomers MAA (b), AM (c), ANA (d) and AAA (e) in acetonitrile. Concentration of KT: 1. 0×10^{-4} mol L^{-1}; Concentration of monomer: 4.0×10^{-4} mol L^{-1}, Corresponding pure monomer solutions as blanks.

above 7.0 was unfavourable to test. On one hand, strong acidity may interferes with hydrogen bonding between template KT and imprinted sites in the membrane. On the other hand, strong alkalinity causes the hydrolysis of probe $K_3Fe(CN)_6$ into $Fe(OH)_3$ precipitation. Therefore, 0.1 mol L^{-1} KCl with 5.0 mmol L^{-1} $K_3Fe(CN)_6$ (pH 6.0) were chosen as buffer solutions.

The incubation time is one of the most important factors that influence the response of the sensor to the targets. The DPV responses at different incubation times were measured using the electrode immersed in 5.0 mmol L^{-1} $K_3Fe(CN)_6$ solutions containing 0.1 mol L^{-1} KCl and 5.0 μmol L^{-1} KT. As shown in Fig. S3, the peak current achieves its minimum value at an incubation time of 5 min, which suggests that the adsorption equilibrium could be obtained within 5 min and that the prepared sensor possesses fast rebinding dynamics.

3.5. Calibration curve

The DPV responses and the calibration curve for the electrochemical determination of KT using the proposed KT-MIM/MOFs@G/SPE under optimal experimental conditions were investigated. It can be seen from Fig. 4 that the peak currents decrease with the increasing KT concentration. The inset in Fig. 4 shows that the change in current (Δi) has a good linear correlation with the logarithm of the KT concentration. The linear regression equation of the calibration curve was obtained as $\Delta i = 13.494 + 2.6274 \log (c, \mu mol\ L^{-1})$ ($R^2 = 0.9963$) in the KT concentration dynamic range over 1.0×10^{-10} – 4.0×10^{-5} mol L^{-1}. Here, $\Delta i = i_0 - i_c$, where i_0 and i_c are the currents for KT concentrations of 0 and c μmol L^{-1}, respectively. The detection limit (LOD) was calculated to be 4.0×10^{-11} mol L^{-1} according to $3S_b/m$, where S_b is the standard deviation of the blank measures and m is the slope of the calibration curve. In comparison to the other techniques (Table 1), the developed method shows a comparatively low detection limit, and a satisfactory dynamic range. This may be attributed to the specific recognition ability of MIM and concentrate template molecules KT on the surface of MIM/MOFs@G/SPE.

3.6. Selectivity, repeatability, and stability of KT-MIM/MOFs@G/SPE

The selectivity of the electrode towards KT was investigated by testing its DPV response to 5.0 μmol L^{-1} KT and with other possible interferences in the samples, such as norketamine (NKT), methylenedioxymethamphetamine (MDMA), methylamphetamine (MA), dopamine (DA), and ascorbic acid (Vc). From Fig. 5 it can be seen that the current response of the sensor towards KT is larger than for the other analytes. This indicates that there is a much greater amount of the template molecules binding to the imprinted film than the other analytes. However, the sensor also shows a good response to NKT since its molecular structure is similar to that of ketamine. Furthermore, the current responses are higher on the imprinted electrode than the non-imprinted electrode, which is due to the specific interaction between the template molecules and the MIM on the electrode surface.

To investigate the reproducibility of the prepared electrode, three KT-MIM/MOFs@G/SPE sensors were investigated in a solution contain 5.0 μmol L^{-1} KT under the same experimental conditions. The relative standard deviation (RSD) of the peak currents obtained using the different sensors was 3.2%. In addition, the RSD of the same sensor for five successive assays was 3.5%. Furthermore, the storage stability of the sensor was also investigated. It was determined that the sensor could retain more than 90% of its original response after being used at least 60 times or stored in a refrigerator for two months. The results demonstrate that the sensor possesses excellent reproducibility and stability.

3.7. Sample analysis

To evaluate the sensors practical applicability, the proposed KT-MIM/MOFs@G/SPE sensor was used to detect KT in the urine and saliva of healthy volunteers. The urine and saliva samples were stored in a refrigerator overnight and diluted 10 fold with deionized water just

Table 1
Comparison of the present method with other electrochemical methods for determination of ketamine.

Electrodes	Methods	Linear range (mol L^{-1})	Limit of detection (mol L^{-1})	Ref.
Anti-Kt/MPA/AuE[a]	EIS	1.0×10^{-12}–1.0×10^{-10}	4.1×10^{-13}	Chen et al. (2013)
KT-TPB/KCSE[b]	Potentiometry	2.5×10^{-6}–1.0×10^{-2}	8.5×10^{-7}	Shawish et al. (2014)
G_4HTD/PtNPs/CPE[c]	DPV	0.1×10^{-6}–2.0×10^{-6}	1.0×10^{-7}	Bagheryan et al.(2013)
Zeo-GO/EμPAD[d]	CV	1.0×10^{-9}–5.0×10^{-6}	1.0×10^{-9}	Narang et al. (2017)
Ket/PAMAM-CDs/GNPs/GCE[e]	Electrochemiluminescence	7.3×10^{-10}–7.3×10^{-7}	2.4×10^{-10}	Li et al. (2015)
MIP/sol-gel/f-MWCNTs @AuNPs/PGE[f]	DPV	1.0×10^{-9}–1.0×10^{-6}	7.0×10^{-10}	Deiminiat et al. (2018)
PM-CE/KTpClPB-PVC[g]	Potentiometry	2.6×10^{-6}–1.0×10^{-2}	7.9×10^{-7}	Li et al. (2013)
KT-MIM/MOFs@G/SPE	DPV	1.0×10^{-10}–4.0×10^{-5}	4.0×10^{-11}	this work

[a] Immunosensor based on anti-ketamine and 3-mercaptopropionic acid modified Au electrode.
[b] Silver ion selective electrode based on ketamine hydrochloride with sodium tetraphenyl borate as electoractive materials.
[c] G-quadruplex structure of human telomeric DNA and platinum nanoparticles modified carbon paste electrode.
[d] Zeolites nanoflakes and graphene-oxide nanocrystals modified electrochemical micro fluidic paper-basedanalytical device.
[e] Glass carbon electrode modified with polyamidoamine-carbon dots, gold nanoparticle and anti-ketamine.
[f] Electropolymerization of molecularly imprinted polymer composed of polytyramine, sol-gel, multiwall carbon nanotubes@gold nanoparticles on pencil graphite electrode.
[g] PVC membrane sensors based on 18-crown-6 (PM-CE) and KTpClPB.

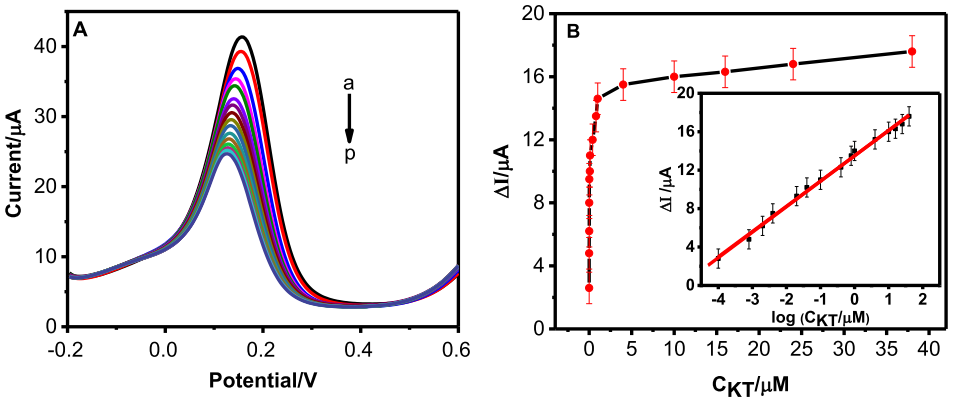

Fig. 4. (A) DPV of KT-MIM/MOFs@G/SPE in 5.0 mmol $L^{-1}K_3Fe(CN)_6$, 0.1 mol L^{-1}KCl and KT of different concentrations (mol L^{-1}). a: 0, b: 1.0×10^{-10}, c: 8.0×10^{-10}, d: 2.0×10^{-9}, e: 4.0×10^{-9}, f: 2.0×10^{-8}, g: 8.0×10^{-8}, h: 1.0×10^{-7}, i: 4.0×10^{-7}, j: 8.0×10^{-7}, k: 1.0×10^{-6}, l: 4.0×10^{-6}, m: 1.0×10^{-5}, n: 1.6×10^{-5}, o: 2.4×10^{-5}, p: 4.0×10^{-5}. (B) The plot of the peak currents difference with KT concentrations ranging from 1.0×10^{-10} to 4×10^{-5} mol L^{-1}. Inset: The calibration curve.

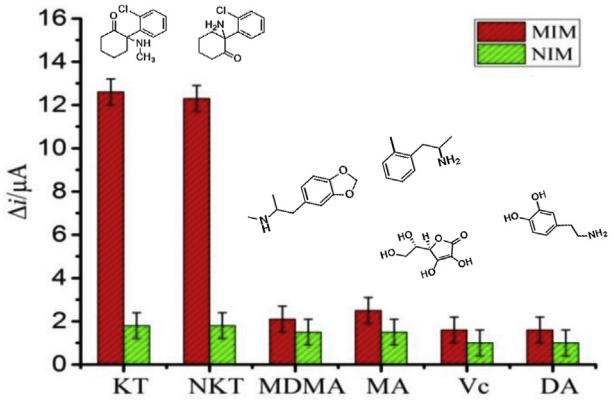

Fig. 5. The peak current response of KT-MIM/MOFs@G/SPE toward 5.0 μmol L^{-1} KT, 5.0 μmol L^{-1} NKT, 20.0 μmol L^{-1} MDMA, 20.0 μmol L^{-1} MA, 20.0 μmol L^{-1} Vc, and 20.0 μmol L^{-1} DA, respectively. The error bars represent the standard deviation of results for $n = 2$.

Table 2
Determination of ketamine in real samples by KT-MIM/MOFs@G/SPE (n = 3).

Samples	Added/μmol L^{-1}	Found/μmol L^{-1}	RSD/%	Recovery/%
	0.05	0.055	3.3	110.0
	0.50	0.56	2.6	112.0
Urine	1.00	0.98	2.5	98.0
	20.00	20.10	1.6	100.5
0.05		0.058	3.0	116.0
Saliva	0.50	0.52	2.5	104.0
	1.00	1.00	2.0	100.0
	20.00	20.10	2.0	100.5

before use. The recovery was determined via the standard addition method. The results are presented in Table 2, the recovery rates of these samples range from 98.0 to 116.0% and the reproducibility expressed as the RSD is less than 3.1%, which indicate that the sensor may be a feasible tool for the determination of KT in real samples.

4. Conclusions

In this study, a novel imprinted electrochemical sensor for the detection of KT based on UV polymerized MIMs on MOFs@G modified screen-printed electrode was developed. The sensor had an ultra-low detection limit (4.0×10^{-11} mol L^{-1}), which could be attributed to the MIM with complementary cavities that could recognize and accumulate the target molecules. Meanwhile, the MOFs@G composite nanomaterial, with its large surface area, could help load the exterior MIM and enhance its electron transfer capability. The proposed electrochemical sensor provides a simple method for the determination of KT with a high sensitivity and selectivity, and good reproducibility and repeatability. Finally, the results of using the sensor in practical detection applications suggested that it could be a promising technique for trace KT detection in urine and saliva samples.

Conflict of interest statement

We declare that we have no financial and personal relationships with other people or organizations that can inappropriately influence our work, there is no professional or other personal interest of any nature or kind in any product, service and/or company that could be construed as influencing the position presented in, or the review of, the manuscript entitled.

CRediT authorship contribution statement

Kaixin Fu: Methodology, Data curation, Formal analysis, Writing - original draft. **Ruilin Zhang:** Data curation, Formal analysis, Writing - review & editing. **Jingcheng He:** Data curation, Writing - original draft. **Genlin Zhang:** Funding acquisition, Project administration, Writing - review & editing.

Declaration of competing interest

The authors declare that they have no known competing financial interests or personal relationships that could have appeared to influence the work reported in this paper.

Acknowledgements

This work was supported by the Natural Science Fund of Yunnan (2017FB012 and 2018FB014).

Appendix A. Supplementary data

Supplementary data to this article can be found online at https://doi.org/10.1016/j.bios.2019.111636.

References

Ahmad, O.S., Bedwell, T.S., Esen, C., Garcia-Cruz, A., Piletsky, S.A., 2019. Trends Biotechnol. 37 (3), 294–309.
Ayankojo, A.G., Reut, J., Öpik, A., Furchner, A., Syritski, V., 2018. Biosens. Bioelectron. 118, 102–107.
Bagheri, N., Khataee, A., Habibi, B., Hassanzadeh, J., 2018. Talanta 179, 710–718.
Bagheryan, Z., Raoof, J.B., Ojani, R., Hamidi-Asl, E., 2013. Electroanalysis 25 (12), 2659–2667.
Bai, H., Wang, C., Chen, J., Peng, J., Cao, Q., 2015. Biosens. Bioelectron. 64, 352–358.
Cavka, J.H., Jakobsen, S., Olsbye, U., Guillou, N., Lamberti, C., Bordiga, S., Lillerud, K.P., 2008. J. Am. Chem. Soc. 130 (42), 13850–13851.
Chen, J., Bai, H., Li, Y., Zhang, J., Liu, P., Cao, Q., 2018. Sens. Actuators B 271, 329–335.
Chen, Y., Yang, Y., Tu, Y., 2013. Sens. Actuators B 183, 150–156.

Deiminiat, B., Rounaghi, G.H., 2018. Sens. Actuators B. 259, 133–141.
El-Naby, E.H., 2014. Anal. Methods 6 (3), 900–906.
Favretto, D., Vogliardi, S., Stocchero, G., Nalesso, A., Tucci, M., Terranova, C., Ferrara, S.D., 2013. Forensic Sci. Int. 226 (1), 88–93.
Furukawa, H., Cordova, K.E., O'Keeffe, M., Yaghi, O.M., 2013. Science 341 (6149), 1230444.
Gam-Derouich, S., Jouini, M., Ben Hassen-Chehimi, D., Chehimi, M.M., 2012. Electrochim. Acta 73, 45–52.
Ghanei-Motlagh, M., Taher, M.A., Heydari, A., Ghanei-Motlagh, R., Gupta, V.K., 2016. Mater. Sci. Eng. C 63, 367–375.
Guo, T., Deng, Q., Fang, G., Gu, D., Yang, Y., Wang, S., 2016. Biosens. Bioelectron. 79, 341–346.
Leung, K.W., Wong, Z.C.F., Ho, J.Y.M., Yip, A.W.S., Ng, J.S.C., Ip, S.P.H., Ng, W.Y.Y., Ho, K.K.L., Duan, R., Zhu, K.Y., Tsim, K.W.K., 2016. Forensic Sci. Int. 259, 53–58.
Li, X., Zhang, L., Wei, X., Li, J., 2013. Electroanalysis 25 (5), 1286–1293.
Li, Q.H., Tang, W.J., Wang, Y., Di, J.W., Yang, J.P., Wu, Y., 2015. J. Solid State Electrochem. 19, 2973–2980.
Lian, K., Zhang, P., Niu, L., Bi, S., Liu, S., Jiang, L., Kang, W., 2012. J. Chromatogr. A 1264, 104–109.
Liu, H., Ni, T., Mu, L., Zhang, D., Wang, J., Wang, S., Sun, B., 2018. Sens. Actuators B 256, 1038–1044.
Maddah, B., Alimardani, V., Moradifard, H., 2015. Anal. Methods 7, 10364–10370.
Moreno, I., Barroso, M., Martinho, A., Cruz, A., Gallardo, E., 2015. J. Chromatogr. B 1004, 67–78.
Narang, J., Malhotra, N., Singhal, C., Mathur, A., Chakraborty, D., Anil, A., Ingle, A., Pundir, C.S., 2017. Biosens. Bioelectron. 88, 249–257.
Peng, Y., Gautam, L., Hall, S.W., 2019. Chemosphere 223, 438–447.
Porpiglia, N., Musile, G., Bortolotti, F., De Palo, E.F., Tagliaro, F., 2016. Forensic Sci. Int. 266, 304–310.
Ramiole, C., D'Hayer, B., Boudy, V., Legagneux, J., Fonsart, J., Houzé, P., 2017. J. Pharm. Biomed. Anal. 146, 369–377.
Shawish, H.M.A., Saadeh, S.M., Tamos, H., Abed-Almonem, K.I., khalili, O.A., 2014. Anal. Chem. Res. 2, 30–36.
Shawish, H.M.A., Tamous, H., Saadeh, S.M., Abed-Almonem, K.I., 2015. Mater. Sci. Eng. C 49, 445–451.
Taniselass, S., Arshad, M.K.M., Gopinath, S.C.B., 2019. Biosens. Bioelectron. 130, 276–292.
Theurillat, R., Knobloch, M., Schmitz, A., Lassahn, P.G., Mevissen, M., Thormann, W., 2007. Electrophoresis 28, 2748–2757.
Yang, Y., Zhai, S.Y., Liu, C., Wang, X.S., Tu, Y.F., 2019. ACS Omega 4, 801–809.
Zhang, X.F., Wang, Z., Feng, Y., Zhong, Y., Liao, J., Wang, Y., Yao, J., 2018. Fuel 234, 256–262.